

EUV irradiation of exoplanet atmospheres occurs on Gyr timescales

George W. King^{1,2}★ and Peter J. Wheatley^{1,2}†

¹Department of Physics, University of Warwick, Gibbet Hill Road, Coventry, CV4 7AL, UK

²Centre for Exoplanets and Habitability, University of Warwick, Gibbet Hill Road, Coventry, CV4 7AL, UK

Accepted XXX. Received YYY; in original form ZZZ

ABSTRACT

Exoplanet atmospheres are known to be vulnerable to mass loss through irradiation by stellar X-ray and extreme-ultraviolet emission. We investigate how this high-energy irradiation varies with time by combining an empirical relation describing stellar X-ray emission with a second relation describing the ratio of Solar X-ray to extreme-ultraviolet emission. In contrast to assumptions commonly made when modelling atmospheric escape, we find that the decline in stellar extreme-ultraviolet emission is much slower than in X-rays, and that the total extreme-ultraviolet irradiation of planetary atmospheres is dominated by emission after the saturated phase of high energy emission (which lasts around 100 Myr after the formation of the star). Furthermore, we find that the total combined X-ray and extreme-ultraviolet emission of stars also occurs mostly after this saturated phase. Our results suggest that models of atmospheric escape that focus on the saturated phase of high-energy emission are over-simplified, and when considering the evolution of planetary atmospheres it is necessary to follow EUV-driven escape on Gyr timescales. This may make it more difficult to use stellar age to separate the effects of photoevaporation and core-powered mass-loss when considering the origin the planet radius valley.

Key words: X-rays: stars – planet-star interactions

1 INTRODUCTION

X-ray and extreme-ultraviolet (EUV; together, XUV) radiation is thought to be important in driving atmospheric escape from planets and exoplanets (e.g. Watson et al. 1981; Schneider et al. 1998; Lammer et al. 2003) and stellar X-ray luminosities are known to decline over a star’s lifetime, as the star spins down due to magnetic braking (as first suggested by Schatzman 1962). For the first 100 Myr or so, when the star is rapidly rotating, the X-ray emission appears independent of rotation period and is described by an approximately constant ratio of X-ray and bolometric luminosities, $L_X/L_{\text{bol}} \approx 10^{-3}$. During this interval the high energy emission is considered to be *saturated*. This saturated interval is followed by a power law decrease in L_X/L_{bol} , with a power-law index of around -1.1 to -1.4 (Ribas et al. 2005; Jackson et al. 2012). The intense X-ray emission during the saturated phase, followed by the steep decline, has led to a common assumption that the high-energy irradiation of a planetary atmosphere and the resulting atmospheric escape

is dominated by the saturated phase (e.g. Lopez & Fortney 2013; Lammer et al. 2014; Owen & Wu 2017). Indeed, as pointed out by Owen & Wu (2017), a power-law decline significantly steeper than -1 would imply that the total high-energy emission of the star is dominated by the saturated phase.

EUV fluxes for most stars are impossible to measure due to strong interstellar absorption in this waveband, and typically it is assumed that the EUV irradiation of planetary atmospheres declines at the same rate as in X-rays (e.g. Owen & Jackson 2012; Owen & Wu 2013; Jin et al. 2014; Kurokawa & Nakamoto 2014; Luger & Barnes 2015; Ginzburg et al. 2016; Fossati et al. 2017; Owen & Wu 2017; Fleming et al. 2019; Rogers & Owen 2020). However, studies of high-energy Solar observations by Chadney et al. (2015) and King et al. (2018) have noted that Solar EUV emission remains relatively strong as X-ray surface flux decreases. Extrapolation of this Solar relation to higher activity levels successfully reproduces the observed X-ray to EUV flux ratios of nearby active stars (Chadney et al. 2015; King et al. 2018) and the same relation predicts EUV fluxes of exoplanet host stars that are consistent with those extrapolated from Lyman- α observations (Ehrenreich et al. 2015;

★ E-mail: g.king.7@warwick.ac.uk

† E-mail: p.j.wheatley@warwick.ac.uk

Table 1. Power law indices describing the decline in time of stellar X-ray and EUV luminosities as a function of $B - V$ colour. X-ray indices are taken from Jackson et al. (2012) and EUV indices are calculated using the empirical Solar relation from King et al. (2018). The boundary between X-ray and EUV wavebands is taken to be 0.1 keV.

Group	$(B - V)$ colour bin	X-ray index α	Full EUV index $\alpha(\gamma + 1)$	Hard EUV index $\alpha(\gamma_{\text{hard}} + 1)$	Soft EUV index $\alpha(\gamma_{\text{soft}} + 1)$	X-ray ratio [†]	EUV ratio [†]
1	$0.290 \leq (B - V) < 0.450$	-1.22 ± 0.30	-0.70 ± 0.22	$-0.80^{+0.21}_{-0.27}$	$-0.29^{+0.21}_{-0.09}$	2.0 ± 1.6	3.4 ± 1.6
2	$0.450 \leq (B - V) < 0.565$	-1.24 ± 0.19	-0.71 ± 0.17	$-0.81^{+0.15}_{-0.23}$	$-0.30^{+0.20}_{-0.07}$	4.3 ± 2.1	5.6 ± 1.8
3	$0.565 \leq (B - V) < 0.675$	-1.13 ± 0.13	-0.65 ± 0.15	$-0.74^{+0.11}_{-0.19}$	$-0.27^{+0.18}_{-0.20}$	1.7 ± 1.0	3.2 ± 1.1
4	$0.675 \leq (B - V) < 0.790$	-1.28 ± 0.17	-0.74 ± 0.17	$-0.84^{+0.14}_{-0.23}$	$-0.31^{+0.20}_{-0.07}$	2.4 ± 1.6	3.8 ± 1.6
5	$0.790 \leq (B - V) < 0.935$	-1.40 ± 0.11	-0.81 ± 0.17	$-0.92^{+0.12}_{-0.23}$	$-0.33^{+0.23}_{-0.06}$	1.4 ± 0.8	2.8 ± 1.1
6	$0.935 \leq (B - V) < 1.275$	-1.09 ± 0.28	-0.63 ± 0.20	$-0.71^{+0.20}_{-0.25}$	$-0.26^{+0.18}_{-0.06}$	4.2 ± 2.0	5.5 ± 1.8
7	$1.275 \leq (B - V) < 1.410$	-1.18 ± 0.31	-0.68 ± 0.22	$-0.77^{+0.25}_{-0.27}$	$-0.28^{+0.20}_{-0.09}$	3.6 ± 2.0	4.9 ± 1.8

[†] Ratio of the total integrated energy between 100 Myr – 1.0 Gyr and 0 – 100 Myr

Youngblood et al. 2016; Bourrier et al. 2017). This empirical relation between X-ray and EUV fluxes implies that the EUV irradiation of exoplanet atmospheres may decline more slowly in time than X-rays. Consequently, significant EUV-driven atmospheric escape might persist well beyond the saturated phase of high-energy emission.

On-going EUV-driven mass-loss would be important in considering the evolutionary state of individual exoplanets, as well as the exoplanet population as a whole. Indeed, photoevaporation has been suggested to sculpt both the Neptunian desert (Mazeh et al. 2016; Owen & Lai 2018) and the planet radius valley (Fulton et al. 2017; Owen & Wu 2017; Van Eylen et al. 2018). Understanding the time dependence of photoevaporation may allow its effect to be separated from competing processes such as core-powered mass-loss (Ginzburg et al. 2018; Gupta & Schlichting 2019; Berger et al. 2020).

In this letter, we combine empirical relations for the time evolution of stellar X-ray emission with relations for X-ray to EUV flux ratios for the Sun in order to assess the time evolution of the EUV and total XUV irradiation of exoplanet atmospheres.

2 EMPIRICAL STELLAR ACTIVITY RELATIONS

2.1 X-ray flux evolution with time

The evolution in time of average stellar X-ray fluxes is reasonably well defined, including for Sun-like stars by Ribas et al. (2005) and Claire et al. (2012), and for a wider range of spectral types by Jackson et al. (2012). L_X/L_{bol} is seen to evolve with age, t , as

$$\frac{L_X}{L_{\text{bol}}} = \begin{cases} \left(\frac{L_X}{L_{\text{bol}}}\right)_{\text{sat}}, & \text{for } t < t_{\text{sat}}, \\ \left(\frac{L_X}{L_{\text{bol}}}\right)_{\text{sat}} \times \left(\frac{t}{t_{\text{sat}}}\right)^{\alpha}, & \text{for } t > t_{\text{sat}}, \end{cases} \quad (1)$$

where $\left(\frac{L_X}{L_{\text{bol}}}\right)_{\text{sat}}$ is the value of L_X/L_{bol} during the saturation interval, and t_{sat} is the length of that interval, typically around 100 Myr. The power-law indices, α , from Ribas et al. (2005) and Claire et al. (2012) were -1.27 and -1.21 ± 0.50 respectively, and the values from Jackson et al. (2012) are reproduced in Table 1. It is worth noting that most of these

power-law indices are only marginally steeper than -1 , implying that significant X-ray emission is to be expected beyond the saturated interval.

The hard end of the EUV spectrum (100–360 Å) was also studied for nearby Sun-like stars by Ribas et al. (2005) and Claire et al. (2012). They found power-law indices of -1.20 and -1.09 ± 0.48 respectively, similar to their values for soft X-rays (20–100 Å). However, the uncertainties are large, and it was not possible to observe the softer end of the EUV (360–920 Å) due to interstellar absorption.

2.2 EUV flux evolution with X-ray flux

The Sun is the only star for which we can study flux variations across the entire EUV spectrum. Analysis by Chadney et al. (2015) showed that the total EUV flux measured with the TIMED/SEE instrument (Woods et al. 2005) declines less steeply than X-ray flux as a function of the surface X-ray flux. They derived an empirical relation of the form

$$\frac{F_{\text{EUV}}}{F_X} = \beta (F_X)^{\gamma}, \quad (2)$$

where β and γ are constants, and F_{EUV} and F_X are the EUV and X-ray surface fluxes respectively. Chadney et al. (2015) also demonstrated that this empirical relation could be extrapolated successfully to more active stars of different spectral types.

In King et al. (2018), we extended the analysis of Chadney et al. (2015) using additional TIMED/SEE data, and by correcting an issue with the estimated uncertainties in some TIMED/SEE data files. We also calculated values of β and γ for different choices of the boundary between X-ray and EUV wavebands in order to match the bandpasses of various X-ray telescopes. The power-law indices we obtained varied in γ between -0.425 ± 0.110 for a 0.1 keV boundary (appropriate for ROSAT-PSPC) and -0.539 ± 0.140 for a 0.243 keV boundary (appropriate for Chandra-ACIS).

The uncertainties in the power-law indices have been estimated by dividing the TIMED/SEE data into 24 equal time intervals (each spanning roughly six months) and fitting individually.

2.3 EUV flux evolution with time

We can use this observed relationship between EUV and X-ray fluxes for the Sun (and verified by comparison with more active stars) to calculate the expected rate of EUV decline in time for the Sun and other stars by combining it with the X-ray time evolution determined by Jackson et al. (2012). By substitution and rearranging Eqn. 2,

$$\frac{L_{\text{EUV}}}{L_{\text{bol}}} = \beta \left(\frac{L_{\text{bol}}}{A} \right)^\gamma \left(\frac{L_X}{L_{\text{bol}}} \right)^{\gamma+1}, \quad (3)$$

where A is the surface area of the star. Substituting for L_X/L_{bol} from Eqn. 1 for the unsaturated regime ($t > t_{\text{sat}}$) gives

$$\frac{L_{\text{EUV}}}{L_{\text{bol}}} = \beta \left(\frac{L_{\text{bol}}}{A} \right)^\gamma \left(\frac{L_X}{L_{\text{bol}}} \right)_{\text{sat}}^{\gamma+1} \left(\frac{1}{t_{\text{sat}}} \right)^{\alpha(\gamma+1)} t^{\alpha(\gamma+1)}. \quad (4)$$

By way of example, taking a Solar-like star ($\alpha = -1.13 \pm 0.13$ from Jackson et al. 2012) and setting the boundary between X-ray and EUV wavebands at 0.1 keV ($\gamma = -0.425 \pm 0.110$ from Section 2.2) the EUV decline in time after the saturated period is described by a power law of index -0.65 ± 0.15 . We present EUV power law indices for all groups of stars from Jackson et al. (2012) in Table 1.

In the upper panel of Fig. 1, we show the time evolution of L_X/L_{bol} and $L_{\text{EUV}}/L_{\text{bol}}$ for a Solar-like star, illustrating the slower decline of EUV emission after the saturated interval. The lower panel of Fig. 1 shows the cumulative energy output in each band, and the total across both. The cumulative plot shows that while the X-ray energy is seen to gradually level off, the corresponding EUV energy continues to increase sharply, even at late times. Only around 10 per cent of the lifetime EUV energy, and 20 per cent of the total XUV energy, is emitted during the first 100 Myr. This suggests that significant EUV-driven atmospheric escape from exoplanets may persist for Gyr timescales, which is much longer than assumed in the theoretical studies highlighted in Section 1.

It is also worth noting here that there is as much X-ray energy emitted between 100 Myr and 1 Gyr as there is in the first 100 Myr. Two-thirds of the lifetime X-ray emission occurs after 100 Myr.

Table 1 shows the power-law index of the EUV decline is shallower than -1 for the full range of FGK spectral types studied by Jackson et al. (2012). Therefore, in all cases we can expect the majority of EUV energy to be emitted on Gyr timescales. Table 1 shows that FGK stars typically emit 3–6 times more EUV radiation between the age of 100 Myr and 1 Gyr than they do during their first 100 Myr.

2.4 The softer the photons, the slower the decline

The rates of decline we find here for the entire EUV band (0.0136–0.1 keV; 124–912 Å) are shallower than those found by Ribas et al. (2005) and Claire et al. (2012) for the harder end of the EUV (100–360 Å). They are also shallower than the slope inferred from coronal models by Sanz-Forcada et al. (2011). A possible explanation for the different slopes is that the rate of EUV decline varies between the observable hard end of the EUV spectrum and the unobservable soft band (which is obscured by interstellar absorption even

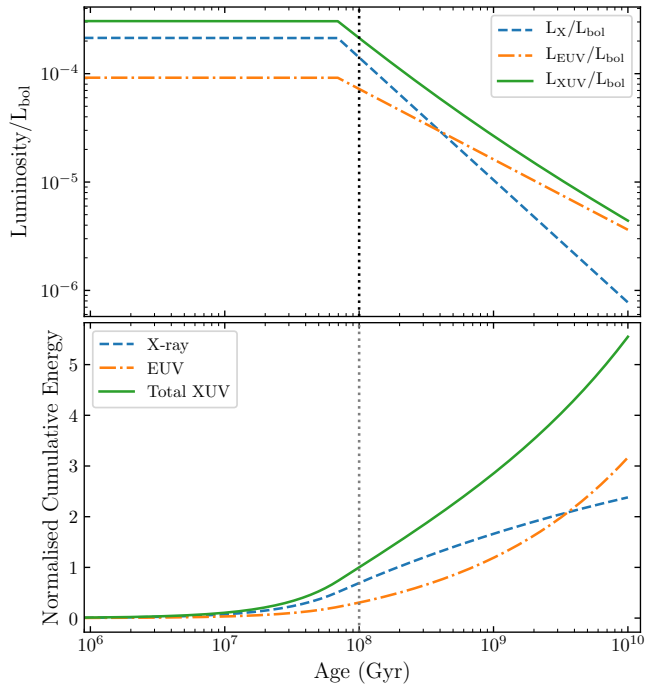


Figure 1. Top panel: Time evolution of the high-energy luminosity of a Sun-like star as determined in Section 2.3. X-ray luminosity is indicated by the dashed blue line, EUV luminosity by the dot-dashed orange line, and the total XUV luminosity by the solid green line. Bottom panel: Cumulative high-energy emission of a Sun-like star in same bands, normalised to the cumulative XUV emission at 100 Myr.

for nearby stars). To investigate this possibility, we reanalysed the Solar *TIMED/SEE* data, separating the hard and soft EUV bands.

Fig. 2 shows the ratio of Solar EUV to X-ray flux, as a function of X-ray surface flux, for both the hard and soft EUV bands as defined by Ribas et al. (2005) and Claire et al. (2012) (100–360 Å, and 360–920 Å). It can be seen that the power-law index is indeed markedly different for these two EUV bands, with $\gamma_{\text{hard}} = -0.35^{+0.07}_{-0.15}$ and $\gamma_{\text{soft}} = -0.76^{+0.16}_{-0.04}$. The associated values of β are 116 and $3040 \text{ erg s}^{-1} \text{ cm}^{-2}$, respectively. In Table 1, we give the implied EUV decline in time for each EUV band and spectral type using the X-ray decline rates from Jackson et al. (2012). For a Solar-type star, we find a time evolution power-law index of $-0.74^{+0.11}_{-0.19}$ for the hard EUV, which is consistent with Ribas et al. (2005) and Claire et al. (2012), and a much shallower slope of $-0.27^{+0.18}_{-0.06}$ for the soft end of the EUV spectrum. This is characteristic of chromospheric activity decline determined by Claire et al. (2012).

3 DISCUSSION

A useful first approximation for the mass loss rate from an exoplanet atmosphere is energy-limited escape (Watson et al. 1981; Erkaev et al. 2007). Here one considers the atmospheric escape to be directly proportional to the input XUV energy, with that energy overcoming gravitational potential energy at some efficiency, typically assumed to be about 15

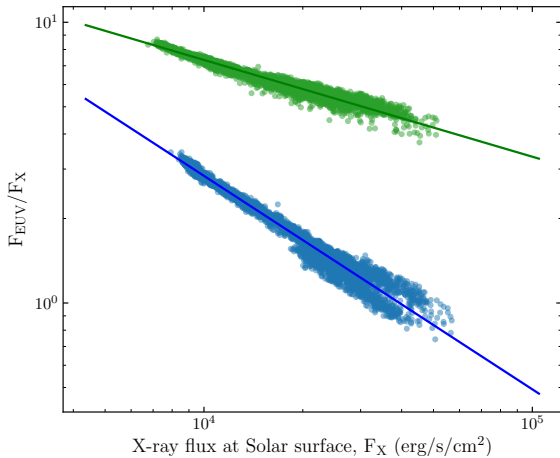


Figure 2. The ratio of Solar EUV to X-ray flux as a function of surface X-ray flux for two different EUV bands, measured using the *TIMED/SEE* instrument. The green data points and power-law fit are for the hard end of the EUV spectrum (100–360 Å), which is observable for nearby stars, while the blue points and power law represent the soft EUV (360–920 Å), which suffers very strong interstellar absorption even for the nearest stars. It is clear that these two EUV bands have different power-law dependence on X-ray flux.

per cent (e.g. Watson et al. 1981; Tian et al. 2005; Kubyshkina et al. 2018). As outlined in Section 1, it is often assumed that the XUV input to the exoplanet atmosphere, and hence its mass loss, is dominated by the saturated phase of stellar activity during the first 100 Myr or so of the lifetime of the star.

The slow decline of EUV emission we infer in Section 2.3 suggests that most high-energy irradiation of exoplanet atmospheres occurs on Gyr timescales, continuing well after the initial 100 Myr (see Fig. 1). We should therefore expect significant evolution of exoplanet atmospheres well beyond the saturated phase of stellar activity. In Table 1 we show that the EUV emission between 100 Myr and 1 Gyr exceeds the emission in the first 100 Myr by factors of 3–6 across spectral types FGK. Furthermore, as can be seen in Fig. 1, the integrated EUV emission continues to increase significantly well beyond 1 Gyr.

Murray-Clay et al. (2009) modelled a hydrodynamic planetary wind from a hot Jupiter and found that simple energy-limited escape is a good approximation when irradiating XUV fluxes are low: $f_{\text{XUV}} < 10^4 \text{ erg s}^{-1} \text{ cm}^{-2}$. In the case of a exoplanet with a semi-major axis of 0.05 au around a Sun-like star, with f_{XUV} following the time evolution in Fig. 1, this condition is satisfied around 800 Myr into the system lifetime. For the higher fluxes at earlier times, a substantial proportion of the input energy is lost to radiative cooling, and atmospheric escape is less efficient (Murray-Clay et al. 2009). Radiative cooling in this “recombination-limited” regime of atmospheric escape therefore further weights mass loss to late times (i.e. even more than the integrated energy flux shown in Fig. 1). The numerical calculations of atmospheric escape from Neptune-mass planets by Ionov et al. (2018) also highlight how energy-limited estimates are a good approximation when irradiating fluxes are low, but that mass loss efficiency is lower for higher irradiating fluxes at earlier times (see their Fig. 3).

Owen & Alvarez (2016) identified a third regime of “photon-limited” atmospheric escape, where the mass loss rate is set by the flux of incoming ionising photons, and which applies at low irradiating fluxes for planets with shallow gravitational potentials. The much slower rate of EUV decline we find for the softest ionising photons (see Section 2.4) implies that photon-limited escape is even further weighted to late times, since the average energy of ionising photons decreases and hence the energetic efficiency of mass loss increases. This softening of the EUV spectrum therefore acts to extend atmospheric escape to even later times for low mass planets.

The correct time-dependence of EUV and XUV irradiation is necessary for understanding the evolution of the exoplanet population as a whole. An important example is the radius valley found between super-Earths and sub-Neptunes with *Kepler* (Fulton et al. 2017; Van Eylen et al. 2018). This had been predicted to arise due to atmospheric escape of primordial H/He envelopes driven by intense XUV irradiation during the saturated phase of stellar activity (Owen & Wu 2013; Lopez & Fortney 2013; Owen & Wu 2017). However, as an alternative explanation, Ginzburg et al. (2018) and Gupta & Schlichting (2019) have shown that the luminosity of the cooling planetary core is also sufficient to strip primordial H/He envelopes, and that this process also leads naturally to a bimodal distribution of planet radii. One way to unravel the relative importance of XUV irradiation and core cooling in sculpting the radius valley is to consider the time-dependence of atmospheric escape, i.e. testing mass-loss predictions against populations of planets selected by age (Berger et al. 2020). Core-powered mass loss will occur on timescales of Gyr (Ginzburg et al. 2018; Gupta & Schlichting 2019), whereas it has been expected that photoevaporation will be dominated by the first 100 Myr (Lopez & Fortney 2013; Lammer et al. 2014; Owen & Wu 2017; Rogers & Owen 2020). Our results suggest that photoevaporation may act on longer timescales than has generally been considered.

In this work, we have assumed the X-ray-age relations of Jackson et al. (2012) as a basis to consider how the EUV and total XUV fluxes evolve with time. However, there are indications that X-ray evolution in time may be more complex than found by Jackson et al. (2012). For example, Tu et al. (2015) suggested that a range of initial stellar spin periods leads to some stars spending much longer in the saturated phase than others (a range of 20–500 Myr, instead of the canonical 100 Myr). This range of stellar spin histories will lead to greater scatter in the integrated X-ray, EUV and total XUV emission plotted in Fig. 1, however, our conclusion that the slow decline of EUV flux leads to late-time evolution of exoplanet atmospheres is unaffected. Indeed, for stars that form with relatively slow initial rotation, the integrated EUV emission after the saturated phase will be an even greater proportion of the lifetime XUV emission.

For older stars, Booth et al. (2017) found evidence that the X-ray power-law decline may steepen beyond at an age of around 1 Gyr. This might reduce the importance of atmospheric escape at later times. However, as the authors state, confirmation of this result requires further work with a large sample of stars. Even if this late-time steep decline is confirmed, our conclusion that the EUV emission between

0.1–1 Gyr greatly exceeds the saturated phase is unaffected (see Table 1).

4 CONCLUSIONS

In this letter we have considered how stellar EUV emission varies with stellar age. By combining empirical relations for stellar X-ray emission with empirical relations for Solar EUV to X-ray ratios, we find evidence that stellar EUV emission declines in time with power-law indices substantially shallower than -1 (see Table 1). This implies that significant EUV irradiation of exoplanet atmospheres continues on Gyr timescales, and that the resulting photoevaporation is not dominated by the saturated activity phase during the first 100 Myr (see Fig. 1). For instance, we find that EUV emission in the interval 0.1–1 Gyr exceeds emission during the first 100 Myr by a factor 3–6 (see Table 1).

We note that total EUV-driven mass-loss is weighted further to late times by the known decrease in photoevaporation efficiency with irradiating flux (in the recombination-driven regime). In addition, we also find that the EUV spectrum softens significantly during the decline, which increases the flux of ionising photons for a given energy flux. This weights EUV-driven mass loss to even later times in the photon-limited regime for planets with shallow gravitational potentials.

While our results rely on the assumption that spectral variations observed for the Solar corona are characteristic of the long-term spectral evolution of stellar coronae, our approach has the advantage of being entirely empirical, with no need to employ poorly-constrained coronal models or to attempt to extrapolate X-ray spectra to the EUV waveband. Previous work has also shown that this approach successfully reproduces X-ray to EUV ratios of nearby active stars (Chadney et al. 2015; King et al. 2018) and that our EUV estimates that are consistent with extrapolations from Lyman- α (Ehrenreich et al. 2015; Youngblood et al. 2016; Bourrier et al. 2017).

Our results strongly suggest that models of atmospheric escape need to account for EUV irradiation that is dominated by Gyr timescales, and not just the first 100 Myr of the life of the system. This will be important in unravelling the relative roles played by photoevaporation and core-powered mass-loss in sculpting features of the exoplanet population such as the radius valley.

ACKNOWLEDGEMENTS

The work presented here was supported by STFC consolidated grants ST/P000495/1 and ST/T000406/1.

REFERENCES

Berger T. A., Huber D., Gaidos E., van Saders J. L., Weiss L. M., 2020, arXiv e-prints, p. arXiv:2005.14671

Booth R. S., Poppenhaeger K., Watson C. A., Silva Aguirre V., Wolk S. J., 2017, *MNRAS*, **471**, 1012

Bourrier V., Ehrenreich D., King G., Lecavelier des Etangs A., Wheatley P. J., Vidal-Madjar A., Pepe F., Udry S., 2017, *A&A*, **597**, A26

Chadney J. M., Galand M., Unruh Y. C., Koskinen T. T., Sanz-Forcada J., 2015, *Icarus*, **250**, 357

Claire M. W., Sheets J., Cohen M., Ribas I., Meadows V. S., Catling D. C., 2012, *ApJ*, **757**, 95

Ehrenreich D., et al., 2015, *Nature*, **522**, 459

Erkaev N. V., Kulikov Y. N., Lammer H., Selsis F., Langmayr D., Jaritz G. F., Biernat H. K., 2007, *A&A*, **472**, 329

Fleming D. P., Barnes R., Luger R., VernerPlas J. T., 2019, arXiv e-prints, p. arXiv:1906.05250

Fossati L., et al., 2017, *A&A*, **598**, A90

Fulton B. J., et al., 2017, *AJ*, **154**, 109

Ginzburg S., Schlichting H. E., Sari R., 2016, *ApJ*, **825**, 29

Ginzburg S., Schlichting H. E., Sari R., 2018, *MNRAS*, **476**, 759

Gupta A., Schlichting H. E., 2019, *MNRAS*, **487**, 24

Ionov D. E., Pavlyuchenkov Y. N., Shematovich V. I., 2018, *MNRAS*, **476**, 5639

Jackson A. P., Davis T. A., Wheatley P. J., 2012, *MNRAS*, **422**, 2024

Jin S., Mordasini C., Parmentier V., van Boekel R., Henning T., Ji J., 2014, *ApJ*, **795**, 65

King G. W., et al., 2018, *MNRAS*, **478**, 1193

Kubyshkina D., et al., 2018, *A&A*, **619**, A151

Kurokawa H., Nakamoto T., 2014, *ApJ*, **783**, 54

Lammer H., Selsis F., Ribas I., Guinan E. F., Bauer S. J., Weiss W. W., 2003, *ApJ*, **598**, L121

Lammer H., et al., 2014, *MNRAS*, **439**, 3225

Lopez E. D., Fortney J. J., 2013, *ApJ*, **776**, 2

Luger R., Barnes R., 2015, *Astrobiology*, **15**, 119

Mazeh T., Holczer T., Faigler S., 2016, *A&A*, **589**, A75

Murray-Clay R. A., Chiang E. I., Murray N., 2009, *ApJ*, **693**, 23

Owen J. E., Alvarez M. A., 2016, *ApJ*, **816**, 34

Owen J. E., Jackson A. P., 2012, *MNRAS*, **425**, 2931

Owen J. E., Lai D., 2018, *MNRAS*,

Owen J. E., Wu Y., 2013, *ApJ*, **775**, 105

Owen J. E., Wu Y., 2017, *ApJ*, **847**, 29

Ribas I., Guinan E. F., Güdel M., Audard M., 2005, *ApJ*, **622**, 680

Rogers J. G., Owen J. E., 2020, arXiv e-prints, p. arXiv:2007.11006

Sanz-Forcada J., Micela G., Ribas I., Pollock A. M. T., Eiroa C., Velasco A., Solano E., García-Álvarez D., 2011, *A&A*, **532**, A6

Schatzman E., 1962, *Annales d'Astrophysique*, **25**, 18

Schneider J., Rauer H., Lasota J. P., Bonazzola S., Chassefiere E., 1998, in Rebolo R., Martin E. L., Zapatero Osorio M. R., eds, *Astronomical Society of the Pacific Conference Series Vol. 134, Brown Dwarfs and Extrasolar Planets*. p. 241

Tian F., Toon O. B., Pavlov A. A., De Sterck H., 2005, *ApJ*, **621**, 1049

Tu L., Johnstone C. P., Güdel M., Lammer H., 2015, *A&A*, **577**, L3

Van Eylen V., Agentoft C., Lundkvist M. S., Kjeldsen H., Owen J. E., Fulton B. J., Petigura E., Snellen I., 2018, *MNRAS*, **479**, 4786

Watson A. J., Donahue T. M., Walker J. C. G., 1981, *Icarus*, **48**, 150

Woods T. N., et al., 2005, *Journal of Geophysical Research (Space Physics)*, **110**, A01312

Youngblood A., et al., 2016, *ApJ*, **824**, 101

This paper has been typeset from a TeX/LaTeX file prepared by the author.